Comparison of SIRM and SOM on Microwave Imaging of the Rough Surface

Wei Chien[1], Chien-Ching Chiu[2] and Chang-En Wu[2]

[1]Department of School of Electric and Information Engineering, Qinzhou University, Guangxi Province, 535000, P.R. China
[2]Electrical Engineering Department, Tamkang University, Tamsui, Taiwan 251, R.O.C.

Abstract

In this paper, the source inversion related method (SIRM) and subspace-based optimization method (SOM) to reconstruct the shape and dielectric constant of the rough surface are investigated. The reconstruction of rough surface has been achieved by buried object approach (BOA), which considers the roughness as a series of objects located alternately on both sides of a planar interface between two half space. By calculating the dielectric constant of these buried objects, we can reconstruct the shape of rough surface through the application of the integral equations and the measured scattered field. The inverse scattering problem is transformed into an optimization problem by SIRM and SOM techniques respectively and solved by self-adaptive dynamic differential evolution (SADDE). Simulation results show that both SIRM and SOM methods can get good results by SADDE algorithms. Simulation results also show that the convergence for SOM is better than that for SIRM.

Key Words: Rough Surface, Self-adaptive Dynamic Differential Evolution (SADDE), Subspace-based Algorithm

1. Introduction

The inverse scattering problem has attracted more attention over the last decades due to its widespread application in archaeology, geophysics civil engineering, biomedical monitoring, and nondestructive testing. It aims at the characterization of electromagnetic properties by utilizing measured scattered fields without destruction. Creating images based on the dielectric constant of the object at the microwave frequencies is of increasing interest due to the potential for new and valuable information. The nonionizing and potentially low cost aspects of microwave imaging are also appealing. We can evaluate the properties of the rough surface material without causing damage, since using the microwave detection does not permanently alter the material being inspected. Microwave inspection can also determine the flow or detect the defects inside the object. It is a highly valuable technique that can save money and time.

In the past two decades, rough surface scattering has been intensive studied [1–9]. The microwave imaging for the rough surface has also been investigated in recently ten years [10–14]. A method to reconstruct the rough surface by buried object approach (BOA) and contrast source inversion (CSI) [15,16] has been proposed. BOA considers a rough surface as a series of objects buried in the half space [17]. On the other hand, a subspace-based optimization method (SOM) for inverse scattering has been reported in [18,19]. The SADDE has been widely applied to the electromagnetic optimization problems such as antennas and filters, and is better than the dynamic differential evolution (DDE) [20]. Some applications of SADDE on the inverse scattering have been published during these years [21,22]. However, the recon-

*Corresponding author. E-mail: chiu@ee.tku.edu.tw

struction for the rough surface has not been reported yet by SADDE. Moreover, there are only two different permittivities for the rough surface which are modeled as the buried objects on the planer surface. In other words, the buried objects have only two possible value of permittivities instead of inhomogeneous permittivity distribution. An integer self-adaptive dynamic differential evolution (ISADDE) is proposed to find a better reconstruction image. ISADDE is a new approach to find the correct dielectric constant distribution more efficiently. It reduces a lot of reconstruction time for rough surface. We will use SADDE algorithm combined with contrast source inversion or the subspace-based optimization method to reconstruct the rough surface. To the best of our knowledge, there are no comparison of SIRM and SOM methods by self-adaptive dynamic differential evolution for the rough surface imaging.

This paper focuses on the reconstruction of rough surface by using the SADDE with SIRM or SOM respectively. The reconstruction accuracy and speed of the rough surface by the two inversion methods are compared. Moreover, the anti-noise ability of these two methods are also investigated. In section 2, the theoretical formulation is presented. The inverse scattering problems for SIRM and SOM are formulated in section 3. Section 4 gives numerical results of the proposed inverse problems. The conclusion is given in section 5.

2. Theoretical Formulation

Let us consider a rough space, as shown in Figure 1. The dielectric constants and conductivity in the region 1 and region 2 are (ε_1, σ_1) and (ε_2, σ_2) respectively. The permeability in each region is set to μ_0 (the permeability of the free space). It means only the non-magnetic material is considered. In the paper, buried object approach is used to calculate the scattered fields for the direct and inverse problem. This approach considers the roughness as a series of objects located alternately on both side of a planar interface between two half spaces. As a result, the objects can be regarded as 2-dimensional scatterers. In other words, the scatterers extend indefinitely in the z-axis direction, the properties of the objects vary only with the x and y coordinates, independent of the z axis. Suppose the incident wave with the e^{jwt} of the time harmonic, and set the radio field parallel to the z-axis of a uniform plane wave, i.e. TM (transverse magnetic) [23] polarized wave $\left(\frac{\partial}{\partial z}=0\right)$. E_i is the incident electric field with an incident angle of ϕ, and the electric field distribution is represented by $\vec{E}_i$ when the object does not exist in space, $\vec{E}_i$ can be expressed as

$$E_i(\vec{r})E_i(x,y)\hat{z} \tag{1}$$

where

$$E_i(x,y)=\begin{cases} E_1(x,y)=e^{-jk_1\left[x\sin\phi_1+(y+a)\cos\phi_1\right]} \\ \qquad +R_1e^{-jk_1\left[x\sin\phi_1-(y+a)\cos\phi_1\right]} \\ E_2(x,y)=Te^{-jk_2\left[x\sin\phi_2+(y+a)\cos\phi_2\right]} \end{cases} \tag{2}$$

$$R_1=\frac{1-n}{1+n},\ T=\frac{2}{1+n},\ n=\frac{\cos\phi_2}{\cos\phi_1}\sqrt{\frac{\varepsilon_2-j\frac{\sigma_2}{\omega}}{\varepsilon_1-j\frac{\sigma_1}{\omega}}}$$

The first term in E_1 (x, y) is the so-called incident field E^{inc}. If region 1 and region 2 are lossless media, then ϕ_1 and ϕ_2 respectively represent the incident angle and refraction angle; if region 1 and region 2 are lossy medium, then ϕ_1 and ϕ_2 are complex numbers, and the wave form will be very complicated, its propagation direction and attenuation direction is not the same. The total elec-

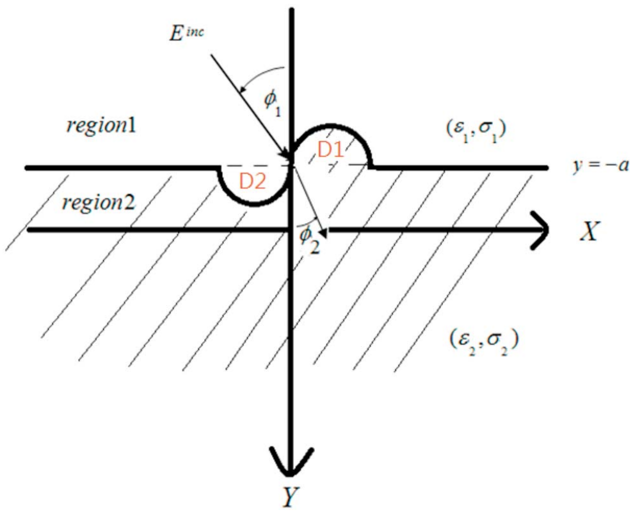

Figure 1. Two-dimensional rough surface in half space.

tric field at any point in space can be expressed

$$E_t(x, y) = \begin{cases} E_1(x, y) + E_s(x, y), \ y \le -a \\ E_2(x, y) + E_s(x, y), \ y > -a \end{cases} \tag{3}$$

where $E_s(x, y)$ is the scattering field.

According to BOA, we treat the rough surface as two objects D1 and D2 buried in the half-space and follow the concept of equivalent induction source, the scattering electric field can be expressed as

$$\begin{aligned} &\overline{E}_s(x, y) = \\ &\iint_{D1} k_1^2 \tau_1 G_1(x, y; x', y') E_t(x', y') dx'dy' + \\ &\iint_{D2} k_2^2 \tau_2 G_2(x, y; x', y') E_t(x', y') dx'dy' \end{aligned} \tag{4}$$

where $G_1(x, y; x', y')$ and $G_2(x, y; x', y')$ are two-dimensional half-space Green's functions which can be expressed as the following integral form

(i) Green's function for the line source in the region 1

$$\begin{aligned} &G_1(x, y, x', y') = \\ &\begin{cases} G_{21}(x, y, x', y'), \ y > -a \\ G_{11}(x, y, x', y') = G_{f11}(x, y, x', y') + G_{s11}(x, y, x', y'), \\ y \le -a \end{cases} \end{aligned} \tag{5}$$

$$G_{21}(x, y; x', y') = \frac{1}{2\pi} \int_{-\infty}^{\infty} \frac{j}{\gamma_1 + \gamma_2} e^{j\gamma 2(y+a)} e^{-j\gamma 1(y'+a)} e^{-j\alpha(x-x')} d\alpha \tag{5-a}$$

$$G_{f11}(x, y; x', y') = \frac{j}{4} H_0^{(2)} \left[k_1 \sqrt{(x-x')^2 + (y-y')^2} \right] \tag{5-b}$$

$$\begin{aligned} &G_{s11}(x, y; x', y') = \\ &\frac{1}{2\pi} \int_{-\infty}^{\infty} \frac{j}{2\gamma_1} \left(\frac{\gamma_1 - \gamma_2}{\gamma_1 + \gamma_2} \right) e^{-j\gamma_1(y+2a+y')} e^{-j\alpha(x-x')} d\alpha \end{aligned} \tag{5-c}$$

where, $\gamma_i^2 = k_i^2 - \alpha^2$, $i = 1, 2$, $\mathrm{Im}(\gamma_i) \le 0$, $y' < -a$.

(ii) Green's function for the line source in the region 2

$$\begin{aligned} &G_2(x, y, x', y') = \\ &\begin{cases} G_{12}(x, y, x', y'), \ y \le -a \\ G_{22}(x, y, x', y') = G_{f22}(x, y, x', y') + G_{s22}(x, y, x', y'), \\ y > -a \end{cases} \end{aligned} \tag{6}$$

$$G_{12}(x, y; x', y') = \frac{1}{2\pi} \int_{-\infty}^{\infty} \frac{j}{\gamma_1 + \gamma_2} e^{j\gamma_1(y+a)} e^{-j\gamma_2(y'+a)} e^{-j\alpha(x-x')} d\alpha \tag{6-a}$$

$$G_{f22}(x, y; x', y') = \frac{j}{4} H_0^{(2)} \left[k_2 \sqrt{(x-x')^2 + (y-y')^2} \right] \tag{6-b}$$

$$\begin{aligned} &G_{s22}(x, y; x', y') = \\ &\frac{1}{2\pi} \int_{-\infty}^{\infty} \frac{j}{2\gamma_2} \left(\frac{\gamma_2 - \gamma_1}{\gamma_2 + \gamma_1} \right) e^{-j\gamma_2(y+2a+y')} e^{-j\alpha(x-x')} d\alpha \end{aligned} \tag{6-c}$$

where, $\gamma_i^2 = k_i^2 - \alpha^2$, $i = 1, 2$, $\mathrm{Im}(\gamma_i) \le 0$, $y' > -a$.

The function $\tau_1(x', y')$ and $\tau_2(x', y')$ are the contrast functions related to object and is defined by

$$\begin{aligned} \tau_1 &= \frac{k_2^2}{k_1^2} - 1 \quad (x', y') \in D_1 \\ \tau_2 &= \frac{k_1^2}{k_2^2} - 1 \quad (x', y') \in D_2 \end{aligned} \tag{7}$$

Note that the contrast function is zero outside the object. Next, we solve the total field by the following equation

$$\begin{aligned} -\overline{E}_i(x, y) = &\iint_{D1} k_1^2 \tau_1 G_1(x, y; x', y') \overline{E}_t(x', y') dx'dy' \\ &+ \iint_{D2} k_2^2 \tau_2 G_2(x, y; x'y') \overline{E}_t(x', y') dx'dy' \\ &- \overline{E}_t(x', y') \end{aligned} \tag{8}$$

For the direct problem, the scattering fields inside the D_1 and D_2 can be first solved by equation (8). Then the scattered field outside the D_1 and D_2 can be found by equation (4).

When solving the inverse scattering problem by numerical methods, the equations (4) and (8) are transformed into a matrix form by the moment methods. First, we divide the dielectric object $D1$ and $D2$ into N_1 and N_2 small enough areas respectively, which must be small enough that the electric field and permittivity of each zone can be regarded as constant. Then we use the pulse function as the base function and the impulse function as the test function in the point matching method. The integral equation (8) is transformed to a matrix equation as follows:

$$-(E_i) = ([L_A][\tau] - I)(E_t) \tag{9}$$

where (E_i) and (E_t) are $(N_1 + N_2)$ vectors. $[L_A]$ is a $(N_1 + N_2) \times (N_1 + N_2)$ matrix, $[\tau]$ and $[I]$ are the $(N_1 + N_2) \times (N_1 + N_2)$ diagonal matrix and identity matrix, respectively. Similarly, the equation (4) can be transform into the following matrix:

$$(E_s) = ([L_B][\tau](E_t), y < -a \tag{10}$$

where (E_s) is a M-element vector, $[L_B]$ is a $M \times (N_1 + N_2)$ matrix. M is the number of the measurement points. For the direct problem, gives the $[\tau]$ matrix, we can calculate the total field by equation (9) and then calculate the scattered field by equation (10) as follows:

$$(E_s^{cal}) = [L_B][\tau]([I]-[L_A][\tau])^{-1}(E_i) \tag{11}$$

3. Inverse Scattering

3.1 SIRM

Source inversion related method (SIRM) uses the equation (8) to obtain the total field by guessing the distribution of the permittivity of the rough surface, and then calculates the scattering field by equation (4). To get the best overall solution, the objective function is defined as:

$$OF1 = \left\{ \frac{1}{M} \sum_{m=1}^{M} \left| E_s^{\exp}(\vec{r}_m) - E_s^{cal}(\vec{r}_m) \right|^2 \Big/ -\left| E_s^{\exp}(\vec{r}_m) \right|^2 \right\}^{\frac{1}{2}} \tag{12}$$

where M is the number of measuring points, $E_s^{cal}(\vec{r}_m)$ is the scattering field calculated by the optimization rule, and $E_s^{\exp}(\vec{r}_m)$ is the measured scattering field.

3.2 SOM

In [24], a subspace-based algorithm is proposed. The subspace-based algorithm decomposes the induced currents into two orthogonally complementary parts: the deterministic part and the ambiguous part. However the deterministic and ambiguous parts of the induced current are different from the physical radiating and non-radiating currents as in [25]. Subspace-based algorithm studies the relationship between the induced current to scattering field and the SVD for the matrix $[L_B]$. The matrix $[L_B]$ can be expressed as by SVD transform $[L_B] = [U][W][V^*]$. Where $[U]$ is the $M \times M$ orthogonal matrix. $[V^*]$ is the complex-conjugate and transpose matrix of $[V]$ with the size $(N_1 + N_2) \times (N_1 + N_2)$. $[W]$ is the $M \times (N_1 + N_2)$ diagonal matrix.

The matrix $[W]$ consists of singular value of the matrix $[L_B]$. It is found that a part of the induced current is proportional to the first L column vector of the right matrix $[V]$ generated by the SVD of thematrix $[L_B]$ [26]. Therefore, the induce current $(I^d) = [\tau](E_t)$ can be expressed as $(I^d) = [V](\alpha)$. The induced current (I^d) can be decomposed into the deterministic part (I^s) which is in the span of the right singular vectors corresponding to the first L leading singular values, and the ambiguous part (I^n) which is retrieved by optimization. The deterministic part of the induced current provides good initial guesses in inverse scattering and the ambiguous part are optimized by the optimization algorithm to find the solution. After the subspace-based decision, the (I^s) is calculated first, according to

$$(I^d) = (I^s) + (I^n) \tag{13}$$

Alternatively,

$$(I^d) = [V^s](\alpha^s) + [V^n](\alpha^n) \tag{14}$$

where V^s is the signal subspace that contains the first L columns of V. V^n is the noise subspace composed of the last M – L columns of V.

We can find

$$\alpha_j^s = \frac{U_j^* \cdot E_s}{w_j}, \; j = 1 \ldots L \tag{15}$$

where w_j is the j-th diagonal value of the matrix $[W]$. L is the total number of singular values that are above a predefined noise-dependent threshold. L serves as a regularization parameter. The choice of L is a consecutive range rather than a single value which makes the subspace-based algorithm more robust against noise than the contemporary methods. By the graph of the singular value w_j with the log scale, wecan make appropriate judgments to choose L. The method of choosing L is mentioned in [27].

When L has been chosen, also represents the subspace-based decision, then (I^s) is determined from (12) and (15) and the field equation error can be defined as:

$$\Delta^{fie} = \left| [L_B] \cdot [V^n] \cdot (\alpha^n) + [L_B] \cdot (I^s) - E_s^{\exp} \right|^2 \tag{16}$$

where $E_s^{\exp}$ is the measured scattered field. From (9), the following can be obtained:

$$(I^d) = [\tau](E_t) = [\tau]\{(E_i) + [L_A](I^d)\} \tag{17}$$

The substitution of $(I^d) = (I^s) + [V^n](\alpha^n)$ into the above equation, and then α^n satisfies the following equations:

$$[A] \cdot (\alpha^n) = (B) \tag{18}$$

where $[A] = [V^n] - [\tau][L_A][V^n]$ and $(B) = [\tau]\{(E_i) + [L_A](I^s)\} - (I^s)$.

Then the least squares method is used to calculate the optimal solution of α^n:

$$(\alpha^n) = ([A^*] \cdot [A])^{-1} \cdot ([A^*] \cdot (B)) \tag{19}$$

The calculated α^n must satisfy the integral equation, so the state equation error can be defined as:

$$\Delta^{sta} = |[A] \cdot (\alpha^n) - (B)|^2 \tag{20}$$

Finally, the total errors can be expressedas:

$$\Delta^{tot} = \frac{\Delta^{fie}}{\left|E_s^{\exp}\right|^2} + \frac{\Delta^{sta}}{\left|I^s\right|^2} \tag{21}$$

where Δ^{tot} is the field equation error plus the state equation error, so the objective function is defined as:

$$OF2 = f(\tau) = (1/2)\sum_{p=1}^{N_i} (\Delta^{tot})^{1/2} \tag{22}$$

where N_i is number of incident waves.

It is worth mentioning here that the objective function of the subspace algorithm is different as that of SIRM. However, both algorithms are determined by satisfying both the field equation and the state equation. The difference is that the SIRM is derived from the state equation and satisfies the field equation. Subspace algorithm is the opposite, first derived from the field equation, and then met the state equation requirement.

3.3 SADDE

The self-adaptive dynamic differential evolution (SADDE) is an extension of the differential evolution. Differential evolution (DE) is a parallel multi-point direct search optimization method proposed by K. Price and R. Storn in 1995 to solve the Chebyshev polynomial fitting problem [28]. The SADDE is to treat each solution as a parameter vector by randomly selecting the vector difference of each set of parameters and multiplying it by an inertial weighting factor to add to the current best solution to produce a perturbation vector, to disturb the current search to the best solution, in order to avoid the problem into the regional extreme. The possible solutions are generated by mating, which may be preserved depending on whether the objective function performance ratio of the possible solution is superior to the old solution. Where the self-adaptation is introduced into the parameters so that the parameters can be self-adjusted and the newly generated parameter vector must be compared to the best parameter vector if the newly generated parameter vector is superior to the best parameter vector. The newly generated parameter vector is selected as the best parameter vector, so the groups in the SADDE are also updated dynamically. Some examples of application is proposed [29,30]. The above SADDE algorithm treats the buried object as the inhomogeneous object to search the solution. Although the buried object approach models the roughness as finite number of buried homogenous objects.

Moreover, there are only two different permittivities for the upper and lower half spaces. As a result, the integer SADDE is proposed to find the suitable solution. The distribution of the permittivities for the buried objects is regard as the bit value “1" or ”0". The bit value “1" or ”0" represents the permittivity ε_1 and ε_2 respectively. The initial distribution is randomly generated and the mutation process as follows:

$$\begin{aligned}(V_j^{k+1})_i &= \\ (X_j^k)_i \oplus [(X_{best}^k)_i \oplus (X_j^k)_i] &\oplus [(X_m^k)_i \oplus (X_n^k)_i]\end{aligned} \tag{23}$$

where “⊕” is exclusive or (XOR) operation. V_j^{k+1} is the trial parameter vector for the $(k+1)$-th generation. X_j^k is the parameter vector of k-th generation and X_{best}^k is the best parameter vector. X_m^k and X_n^k are two randomly selected parameter vectors. Then, during the process of mating and selection, the advantages of the original SADDE are retained, and the efficiency can be greatly improved for searching the correct dielectric constant distribution.

4. Numerical Results

Some numerical examples are given to compare SIRM and SOM methods to reconstruct the simple rough surface by SADDE. The reconstruction ability and robustness of the two algorithm are compared. Moreover, the sensitivities of these algorithms to the noise is also investigated by the numerical simulation. First we consider a plane wave with an amplitude of 1 incident from region 1 to the rough surface, as shown in Figure 1. The frequency of the incident wave was selected to be 1 GHz, i.e., the wavelength was 0.3 m. We consider that the rough surface consists of a lossless medium, i.e. $\sigma_1 = \sigma_2 = 0$. The media in region 1 is air, i.e., $\varepsilon_1 = 8.85 \times 10^{-12}$ S/m. In the words, the upper half-space is assumed to be a free space. The dielectric constant in region 2 is $\varepsilon_2 = 2.56\varepsilon_1$. Note that the regions in D_1 and D_2 are treated as two buried objects by the BOA method. In the experiment, the upper and lower bounds for ε_1 is from 1 to 1.8, and is from 1.9 to 2.8 for ε_2. The number of iterations is set to be 500 for SADDE. In the numerical simulation, we define the relative square root error rate of the dielectric coefficient distribution as the following:

$$err = \left[\sum_{i=1}^{N} \left| \Delta\tau_i \right|^2 \Big/ \sum_{i=1}^{N} \left| \tau_i^{exect} \right|^2 \right]^{\frac{1}{2}} \tag{24}$$

where τ_i^{exact} is the correct value of the dielectric coefficient of the i-th small area, and the $\Delta\tau_i$ is the difference between the reconstructed value and the correct value.

In the first example, two square shape rough surface divided by two 2×2 cells is presented. The population size for SADDE is 100. Three different incident waves, with incident angles 45°, 90°, and 135° are used. The measurement points are distributed with equally spaced from X = -0.23 m to X = 0.19 m, with the line Y = -2m. There are 8 measurement points in the direction of the incident wave, so there are total 24 measurement points in each simulation. With the SOM, after several experimental data, the best value of parameter L is selected as 7. Figure 2 is the original shape and dielectric constant distribution. Figure 3 is the reconstruction result with SIRM. Figure 4 is the reconstruction result with SOM. Based on the above results, it is found that the reconstructed results of the rough surface are good and the relative errors are both less than 1%. Next, we change the dielectric distribution, as shown in Figure 5. Reconstruction results by SIRM are shown in Figure 6. SOM reconstruction results are plotted in Figure 7. The relative error values are both less than 1%. The related errors versus the number of generation are depicted in the Figure 8. It is clear that the convergence for SOM is better than that for SIRM. Next the effect of noise on the reconstructed image is discussed. Different level of Gaussian noise in the measurement scattering field are added in the scattered fields. Five different levels of 0.001%, 0.01%, 0.1%, 1%, 5% noise are used for simulation. The reconstructed errors for SIRM and SOM are shown in Figure 9. It is seen the results for SIRM is better than those for SOM.

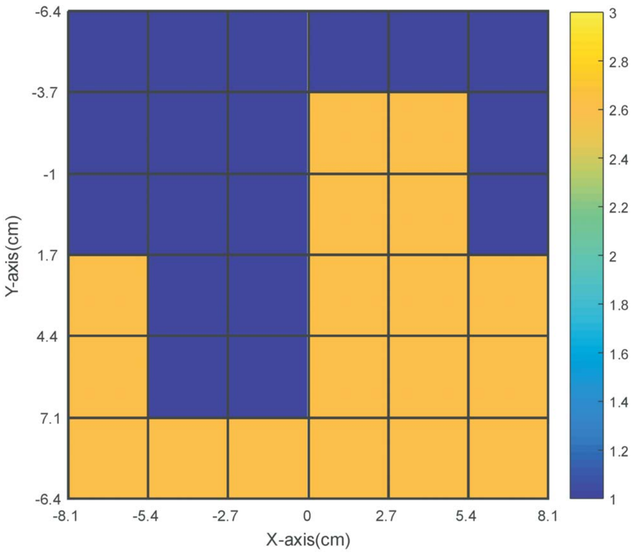

Figure 2. Original shapes for two 2×2 cells.

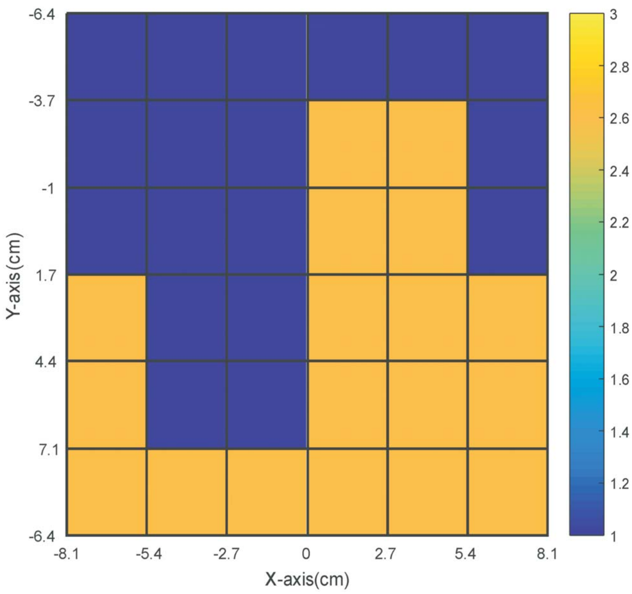

Figure 3. Reconstructed shapes by SIRM.

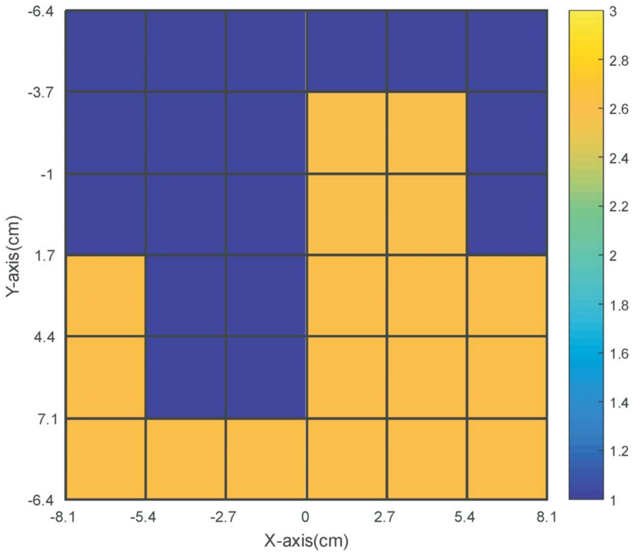

Figure 4. Reconstructed shapes by SOM.

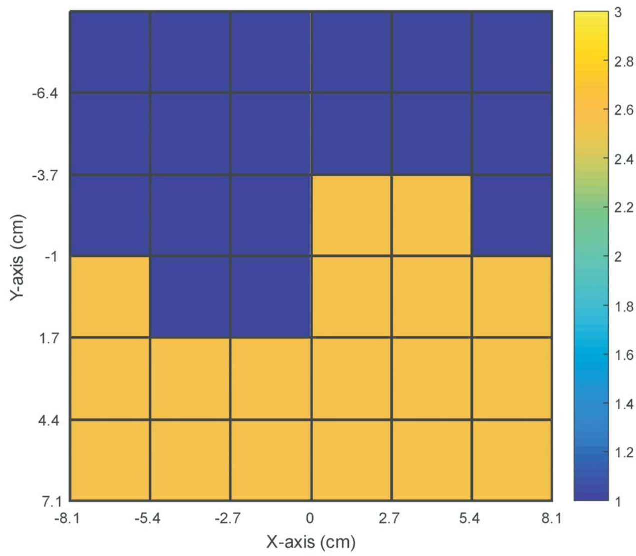

Figure 6. Reconstructed the non-uniform shapes by SIRM.

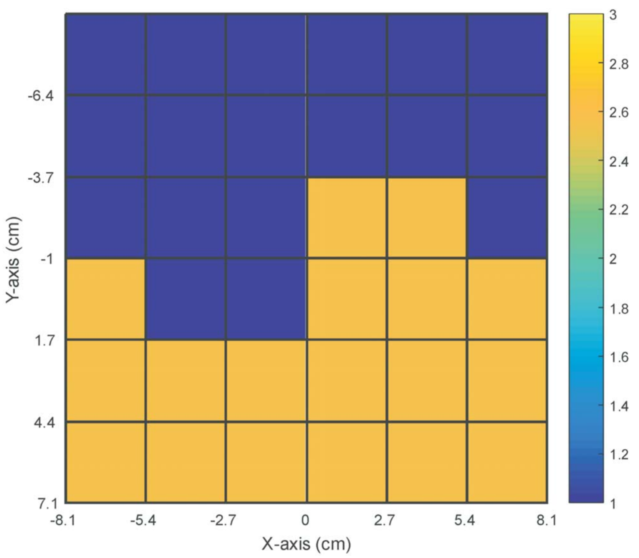

Figure 5. Original non-uniform shapes for two 2×2 cells.

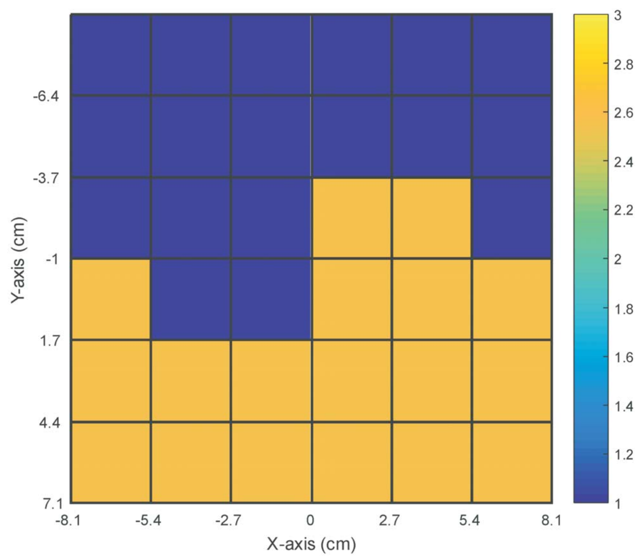

Figure 7. Reconstructed the non-uniform shapes by SOM.

In the second example, two square shape rough surface divided by one 4×4 cells and one 3×3 cells is presented. The population size for SADDE is 150. Three different incident waves, with incident angles 45°, 90°, and 135° are used. The measurement points are distributed with equally spaced from X = -0.35 m to X = 0.31 m, with the line Y = -2m. There are 12 measurement points in the direction of the incident wave, so there are total 36 measurement points in each simulation. With the SOM, after several experimental data, the best value of parameter L is selected as 7. Figure 10 is the original shape and dielectric constant distribution. Figure 11 is the reconstruction result with SIRM. Figure 12 is the reconstruction result with SOM. Based on the above results, it is found that the reconstructed shapes of the rough surface are good and the relative error values are both about 3%. The related errors versus the number of generation are shown in the Figure 13. It is seen that the convergence generation is about 100 and 150 for SOM and SIRM respectively. Next the effect of noise on the reconstructed image is also discussed. Different level of Gaussian noise in the measurement scattering field are

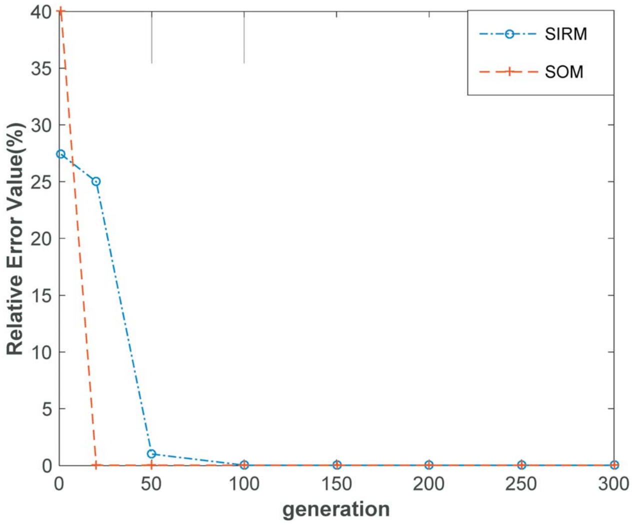

Figure 8. Related errors versus the number of generation.

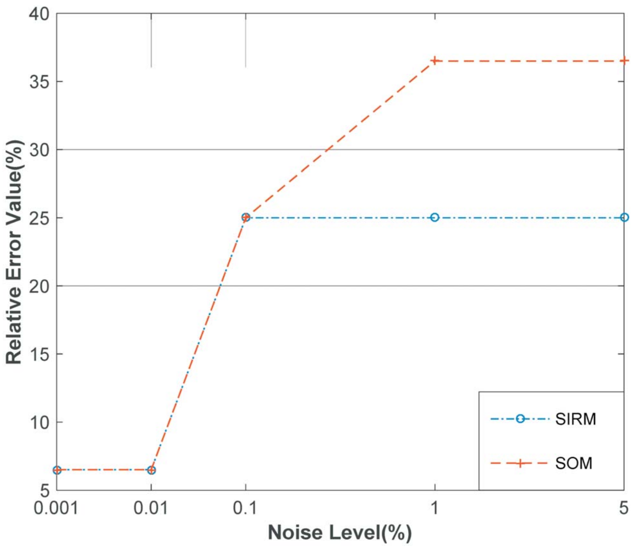

Figure 9. Reactive errors for different noise levels.

added in the scattered fields. Five different levels of 0.001%, 0.01%, 0.1%, 1%, 5% noise are used for simulation. The reconstructed errors for SIRM and SOM are shown in Figure 14. It is seen the results for SIRM is better than those for SOM.

5. Conclusion

In this paper, the problem of reconstructing the rough surface is studied. By using the concept of buried object approach, the complex medium with the rough part can be regarded as a series of objects buried in the flat half

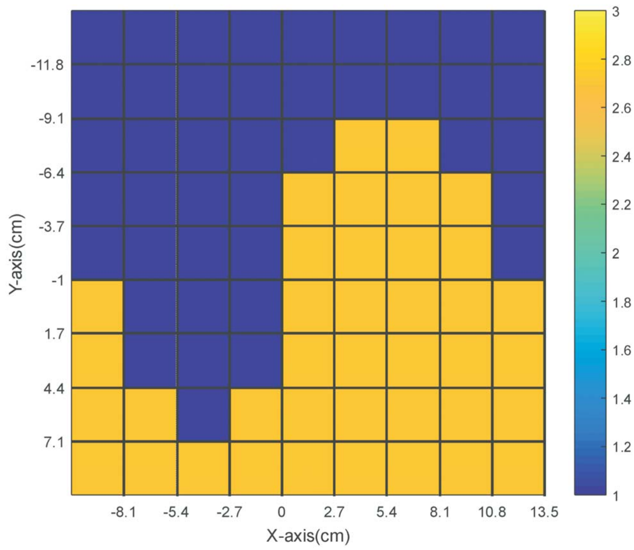

Figure 10. Original shapes for one 4×4 cells and one 3×3 cell.

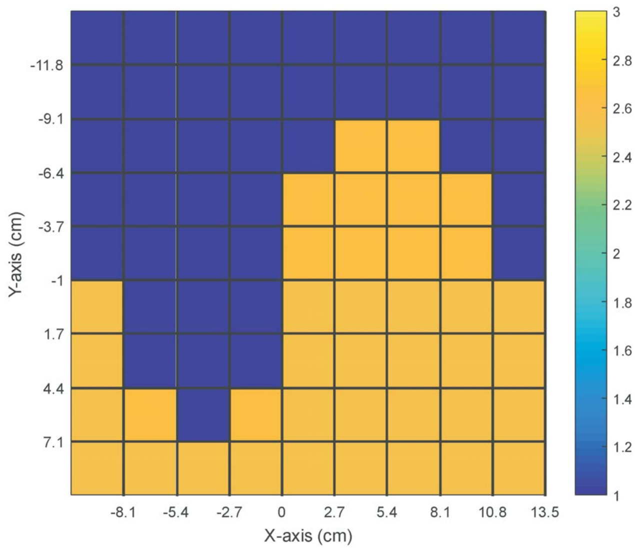

Figure 11. Reconstructed shapes by SIRM.

space. In order to explore the shape of the unknown rough surface, we emit the electromagnetic waves to the surface and record the scattered electromagnetic waves. According to measured scattering fields and the equivalent current concept, a set of nonlinear integral equation and scattering field formula can be derived. In the inverse scattering, the self-adaptive dynamic difference evolution (SADDE) and the integer self-adaptive dynamic difference evolution (ISADDE) is used to reconstruct the imaging with the algorithm of source inversion related method (SIRM) and subspace-based optimiza-

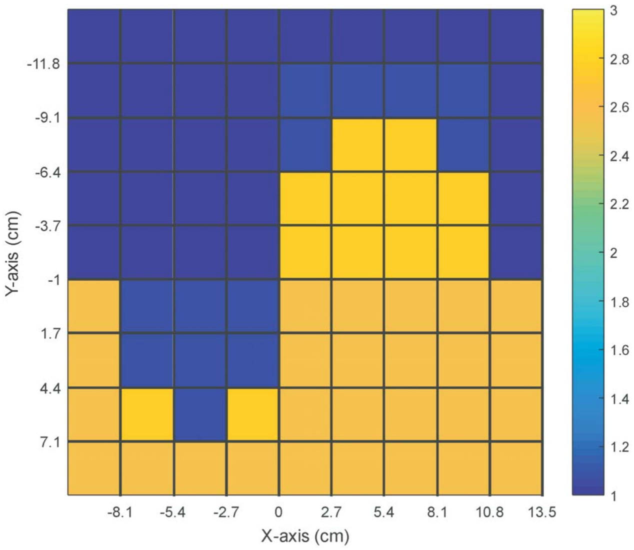

Figure 12. Reconstructed shapes by SOM.

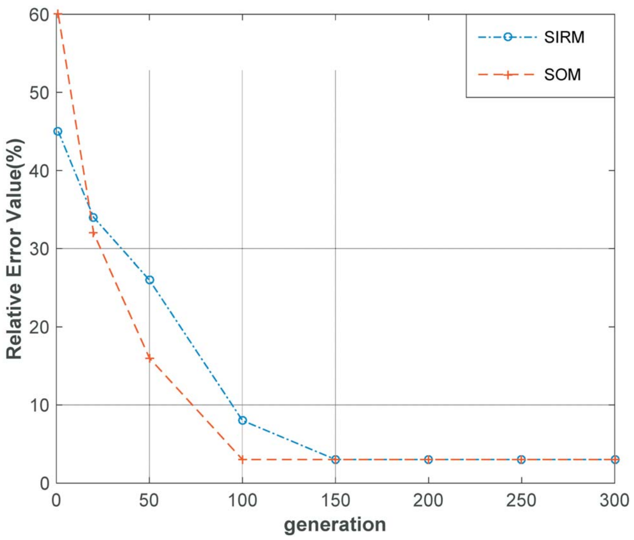

Figure 13. Related errors versus the number of generation.

tion method (SOM), respectively.

In the numerical results, both SIRM and SOM with SADDE can reconstruct the shape and the permittivity of the rough surface. It is found that the ISADDE is very robust and effective to reconstruct the rough surface. We will focus on more complex surface such as periodic and irregular cutting surface, rather than the simples flat surface in the future.

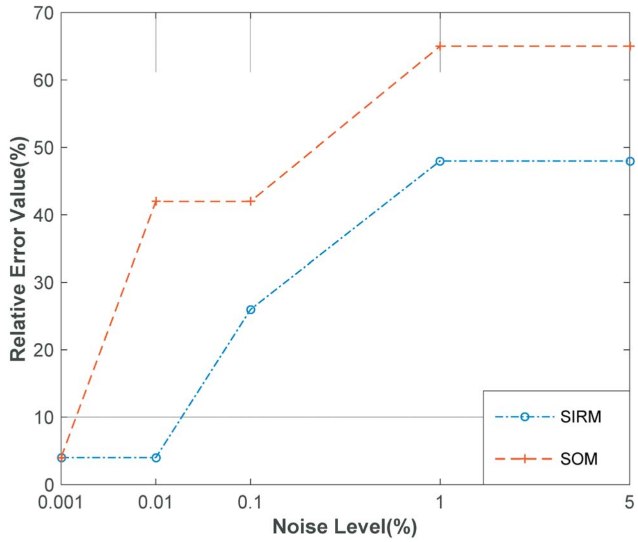

Figure 14. Relative errors for different noise level.

References

[1] DeSanto, J. A., "Exact Spectral Formalism for Rough-surface Scattering," *Journal of the Optical Society of America A*, Vol. 2, pp. 2202–2207 (1985). doi: 10.1364/JOSAA.2.002202

[2] Wombell, R. J. and DeSanto, J. A., "The Reconstruction of Shallow Rough-surface Profiles from Scattered field Data," *Inverse Problems*, Vol. 7, No. 1 (1991). doi: 10.1088/0266-5611/7/1/002

[3] Li, Q., Chan, H. and Tsang, L., "Monte Carlo Simulations of Wave Scattering from Lossy Dielectric Random Rough Surfaces Using the Physics-based Two-grid Method and the Canonical-grid Method," *IEEE Transactions on Antennas and Propagation*, Vol. 47, No. 4, pp. 752–763 (1999). doi: 10.1109/8.768816

[4] Guo, L. X. and Wu, Z. S., "Moment Method with Wavelet Expansions for Fractal Rough Surface Scattering," *Chinese Physics Letters*, Vol. 19, No. 11 (2002). doi: 10.1088/0256-307X/19/11/315

[5] Altuncu, Y., Yapar, A. and Akduman, I., "Numerical Computation of the Green's Function of a Layered Media with Rough Interfaces," *Microw. Opt. Technol. Lett.*, Vol. 49, No. 5, pp. 1204–1209 (2007). doi: 10.1002/mop.22401

[6] Yildiz, S., Altuncu, Y., Yapar, A. and Akduman, I., "On the Scattering of Electromagnetic Waves by Periodic Rough Dielectric Surfaces: a Boa Solution," *IEEE Transactions on Geoscience and Remote Sensing*, Vol. 46, No. 9, pp. 2599–2606 (2008). doi: 10.1109/TGRS.2008.919275

[7] Tezel, N. S., "Electromagnetic Scattering from Inhomogeneous Impedance Periodic Rough Surfaces by Transform Technique," *Microwave and Optical Technology Letters*, Vol. 51, No. 1, pp. 116–119 (2009). doi: 10.1002/mop.23954

[8] Boix, R. R., Fructos, A. L. and Mesa, F., "Closed-form Uniform Asymptotic Expansions of Green's Functions in Layered Media," *IEEE Trans. Antennas Propag.*, Vol. 58, No. 9, pp. 2934–2945 (2010). doi: 10.1109/TAP.2010.2052569

[9] Zamani, H., Tavakoli, A. and Dehmollaian, M., "Scattering from Layered Rough Surfaces: Analytical and Numerical Investigations," *IEEE Transactions on Geoscience and Remote Sensing*, Vol. 54, pp. 3685–3696 (2016). doi: 10.1109/TGRS.2016.2524639

[10] Yapar, A., Ozdemir, O., Sahinturk, H. and Akduman, I., "A Newton Method for the Reconstruction of Perfectly Conducting Slightly Rough Surface Profiles," *IEEE Transactions on Antennas and Propagation*, Vol. 54, No. 1, pp. 275–279 (2006). doi: 10.1109/TAP.2005.861513

[11] Akduman, I., Kress, R. and Yapar, A., "Iterative Reconstruction of Dielectric Rough Surface Profiles at Fixed Frequency," *Inverse Problems*, Vol. 22, No. 3 (2006). doi: 10.1088/0266-5611/22/3/013

[12] Gürbüz, T., Aslanyürek, B., Karabulut, E. P. and Akduman, I., "An Efficient Nonlinear Imaging Approach for Dielectric Objects Buried under a Rough Surface," *IEEE Transactions on Geoscience and Remote Sensing*, Vol. 52, No. 5, pp. 3013–3022 (2014). doi: 10.1109/TGRS.2013.2268662

[13] Shamsaddini, M., Tavakoli, A. and Dehkhoda, P., "Inverse Electromagnetic Scattering of a Dielectric Cylinder Buried below a Slightly Rough Surface Using a New Intelligence Approach," Iranian Conference on Electrical Engineering (ICEE), May (2015). doi: 10.1109/IranianCEE.2015.7146246

[14] Roy, D. G. and Mudaliar, S., "Domain Derivatives in Dielectric Rough Surface Scattering," *IEEE Transactions on Antennas and Propagation*, Vol. 63, pp. 4486–4495 (2015). doi: 10.1109/TAP.2015.2463682

[15] Van Den Berg, P. M. and Kleinman, R. E., "A Contrast Source Inversion Method," *Inverse Problems*, Vol. 13, No. 6, pp. 1607–1620 (1997). doi: 10.1088/0266-5611/13/6/013

[16] Van Den Berg, P. M., Van Broekhoven, A. and Abubakar A., "Extended Contrast Source Inversion," *Inverse Problems*, Vol. 15, No. 5, pp. 1325–1344 (1999). doi: 10.1088/0266-5611/15/5/315

[17] Altuncu, Y., Yapar, A. and Akduman, I., "Numerical Computation of the Green's Function of a Layered Media with Rough Interface," *Microw. Opt. Technol. Lett.*, Vol. 49, No. 5, pp. 1204–1209 (2007). doi: 10.1002/mop.22401

[18] Xu, K., Zhong, Y., Song, R., Chen, X. and Ran, L., "Multiplicative-regularized FFT-twofold Subspace-based Optimization Method for Inverse Scattering Problems," *IEEE Transactions on Geoscience and Remote Sensing*, Vol. 53, pp. 841–850 (2015). doi: 10.1109/TGRS.2014.2329032

[19] Ye, X., Zhong, Y. and Chen, X., "Reconstructing Perfectly Electric Conductors by the Subspace-based Optimization Method with Continuous Variables," *Inverse Problems*, Vol. 27, No. 5, pp. 1–14 (2011). doi: 10.1088/0266-5611/27/5/055011

[20] Li, C. L., Chien, W., Huang, C. H. and Chiu, C. C., "Time Domain Microwave Imaging for a Buried Dielectric Cylinder by Dynamic Differential Evolution," *International Journal of Applied Electromagnetics and Mechanics*, Vol. 34, No. 1, 2, pp. 73–86 (2010). (EI) (SCI).

[21] Wan, Y., Yu, C. Y., Sun, C. H. and Chiu, C. C., "The Reconstruction of Time Domain Through-wall Imaging for a Metallic Cylinder," *Imaging Science Journal*, Vol. 63, No. 2, pp. 81–84 (2015). (EI) (SCI). doi: 10.1179/1743131X14Y.0000000084

[22] Lee, Y. H., Cheng, Y. T., Chiu, C. C. and Chang, S. P., "Microwave Imaging for Half-space Imperfect Conductors," *Nondestructive Testing and Evaluation*, Vol. 30, No. 1, pp. 49–62 (2015). (EI) (SCI). doi: 10.1080/10589759.2014.992430

[23] Wang, X., Gan, Y. B. and Li, L. W., "Electromagnetic Scattering by Partially Buried PEC Cylinder at the Dielectric Rough Surface Interface: TM Case," *IEEE Antennas and Wireless Propagation Letters*, Vol. 2 (2003). doi: 10.1109/LAWP.2003.822200

[24] Chen, X., "The Role of Regularization Parameter of Subspace-based Optimization Method in Solving Inverse Scattering Problems," IEEE Microwave Conference on Asia Pacific, pp. 1549–1552, 7–10 Dec. (2009).

doi: 10.1109/APMC.2009.5384411

[25] Habashy, T. M., Oristaglio, M. L. and De Hoop, A. T., “Simultaneous Nonlinear Reconstruction of 2-dimensional Permittivity and Conductivity,” *Radio Science*, Vol. 29, pp. 1101–1118 (1994). doi: 10.1029/93RS03448

[26] Press, W. H., Teukolsky, S. A., Vetterling, W. T. and Flannery, B. P., *Numerical Recipes in FORTRAN*, Second Edition, The Press Syndicate of the University of Cambridge (1992).

[27] Chen, X., “Subspace-based Optimization Method for Solving Inverse Scattering Problems,” *IEEE Transactions on Geoscience and Remote Sensing*, Vol. 48, pp. 42–49 (2010). doi: 10.1109/TGRS.2009.2025122

[28] Storn, R. and Price, K., “Differential Evolution - a Simple and Efficient Adaptive Scheme for Global Optimization over Continuous Spaces,” Technical Report TR-95-012, International Computer Science Institute, Berkeley (1995).

[29] Sun, C. H. and Chiu, C. C., “Inverse Scattering of Dielectric Cylindrical Target Using Dynamic Differential Evolution and Self-adaptive Dynamic Differential Evolution,” *International Journal of RF and Microwave Computer-Aided Engineering*, Vol. 23, No. 5, pp. 579–585 (2013). doi: 10.1002/mmce.20692

[30] Chiu, C. C., Sun, C. H., Li, C. L. and Huang, C. H., “Comparative Study of Some Population-based Optimization Algorithms on Inverse Scattering of a Two-dimensional Perfectly Conducting Cylinder in Slab Medium,” *IEEE Transactions on Geoscience and Remote Sensing*, Vol. 51, pp. 2302–2315 (2013). doi: 10.1109/TGRS.2012.2208756

Manuscript Received: Nov. 14, 2017
Accepted: Apr. 16, 2018

Charge Policy

To help defray the rising cost of publication and improve the quality of JASE, some page charge is required for publishing accepted papers.

- The first 8 proof pages including figures, tables and others are charged at US$100 or NTD$3000 for each paper which was accepted after June 1, 2018. Two hardcopies of JASE and the PDF file will be respectively sent to the corresponding author after the official publication.
- For the subsequent pages after eight, the authors will be charged at US $65/per page or NTD $2000/per page.